Design of an Accurate Yet Low-Cost Distributed Module for Vehicular Relative Positioning: Hardware Prototype Design and Algorithms

Xinzuo Wang and Wei Li, *Senior Member, IEEE*

Abstract—In this paper, we design a modular prototype to provide relative position and orientation (RPO), with higher accuracy yet low-cost implementations. First, we design the hardware module as two distributed sub-modules: the beacon module and the receiver module. The beacon module is designed to have the rotational laser-emitting function and the wireless-broadcasting function, and the receiver module can receive both the laser signals and wireless broadcasting. Then, with these functions, we design the unique operating mechanisms for the whole module. Finally, we provide the event-triggered algorithms for the RPO measurements, which are tightly incorporated with the hardware design. Compared via experiments with other related methods, our design has more measurement capabilities, higher accuracy, and low-cost implementations on both hardware and computations. This module has potential vehicular applications, e.g., in a factory for tasks assistance.

Index Terms—Beacon module, localization, measurement, modular design, positioning algorithm, vehicular positioning.

I. INTRODUCTION

POSITIONING has a wide range of applications, e.g., positioning of vehicular robots in an automatic factory, path or trajectory tracking, and motion planning [1]–[4], [23], [27], [29], [30] of vehicles. In these applications, knowledge of relative positions and orientations of vehicles are essential.

There are two major types of techniques for positioning: absolute positioning and relative positioning. One example of absolute positioning is the global positioning system (GPS) [5], but the GPS has signal blockage in GPS-denied areas, such as indoor and underground environments. Most techniques are for relative positioning.

For positioning sensors, relative positioning sensors include vision sensors, received signal strength indicators (RSSIs), and proximity sensors. Vision techniques are generally computationally intensive [6]–[11]. RSSIs have relatively low accuracy [12]–[14]. The most widely used proximity sensors include

ultrasonic sensors [15]–[18], infrared sensors [19]–[21], and laser sensors [22]–[26] (such as laser range finders (LRFs) [24], [25]). Ultrasonic sensors cannot provide directional information. For infrared sensors, the effective ranges are short, often with color affection by objects [19]. The valuable features of LRFs are high accuracy and high directionality; however, they are generally very expensive, compared to ultrasonic and infrared sensors. Many relative positioning methods use one or more reference beacons, e.g., as in [4], [7], [15]–[18], [22], [24], and [25].

In this paper, we design a distributed module to provide relative position and orientation (RPO) in an event-triggered manner [6], with high accuracy and low costs of implementations. Here, we discriminate *relative position* (RP) and *relative distance* (RD), that is, a RP is a vector, while a RD is a scalar.

The hardware module we designed consists of two integrated sub-modules: the beacon module and the receiver module. The beacon module has the rotational laser-emitting function and the wireless-broadcasting function. The receiver module can receive both the laser signals and wireless broadcasting.

The laser-emitter is mounted on the top of the beacon module and can rotate horizontally at a designated angular velocity. The receiver module, with three laser-receivers, measures directly the RD relative to the beacon module. The wireless broadcasting and receiving functions help to measure the polar angle and the orientation of the receiver module in the reference coordinates carried by the beacon. Then, integrated with the design of the unique operating mechanisms for the low-cost hardware module, we provide the event-triggered algorithms for the RPO calculations, which is also low-cost.

The modular system can be extendable by adding more receiver modules, each of which can work that is independent from other receiver modules.

The following shows the features of our design with comparisons of other methods from four aspects:

- *Measurements Capability* (i.e., measurements for RPO, or only for RP or RD measurement),
- *Accuracy Comparison,* for RP, RD, or RPO (if available in other methods),
- *Costs Comparison* (the hardware cost and computational cost),
- *Independence Comparison* (i.e., whether one can determine its RPO relative to only one beacon).

The distinct features of our module and the corresponding algorithms are that: it can provide

1) higher accuracy for RPO measurements (not merely for RP measurement),
2) low-cost implementations on both hardware and computations;
3) only one beacon is sufficient for RPO measurements;
4) moreover, there is no necessity on clock synchronization of the MCUs on different modules.

The performances of the measurements are shown as follows:

- For the performance of a single measurement (i.e., without averaging among different measurements), our designed module has the maximum error of 2.0% for RP measurement and 0.9 degree for orientation measurement, at a distance of 200 cm relative to the beacon, which are better than most results reported in previous papers.
- For the average performance of multiple measurements, the average error for RP measurement is only 1.2% (at a distance of 200 cm), and the average error for orientation measurement is only 0.3 degree (at a distance of 200 cm). This is another advantage of our design, since one can easily obtain the high accurate RPO via averaging many measurements within a very short instant, due to both the high rotational velocity of the laser-emitter and the low-cost computations of our module.

Compared with relevant results, for example, the system designed in [19] can only provide RP measurement, with an average error of 2.6% (2.6 cm at 100 cm), in which the algorithm is also computational intensive. The system designed in [20] has the maximum RPO error above 6%. The system in [17] has lower accuracy and low computational efficiency for RPO measurements. The system in [22] can provide only RP measurement relative to a laser beacon with a lower accuracy. The method in [21] requires multiple beacons. Comparisons that are more detailed are provided in Section VI.

The rest of the paper is organized as follows: Section II describes the problem for RPO measurements. Section III designs the hardware. Section IV is the algorithms for the RPO calculations. Section V shows the RPO accuracy via extensive experiments. Section VI compares the performances with relative results. Section VI is the conclusion and future considerations.

II. PROBLEM DESCRIPTION

A. The Pose of a Vehicular Robot

Consider the pose of a vehicular robot as illustrated in Fig. 1, denote v as its heading direction and φ as its orientation, respectively, its pose or configuration is denoted as (x, y, φ), where (x, y) represent the RP. Denote d and θ as the RD and the polar angle, respectively, then

$$x = d\cos\theta, \ y = d\sin\theta.$$

Here a RP is a 2D vector, while a RD is a scalar.

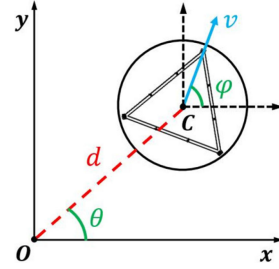Fig. 1. Illustration of the RPO of the robot (its position is denoted as the center C) relative to the beacon O (the beacon carries the x-y reference coordinates).
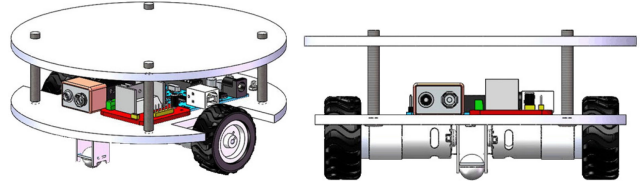

Fig. 2. The vehicular robotic platform prototype (from two different view perspectives), which has two wheels driven by the servomotors, and two omni-directional casters for the stability of the platform. The platform height is 70 mm, the platform radius is 75 mm, and the wheel diameter is 65 mm.

B. Problem Description

Our focus in this paper is two-folds:

1) design a hardware module, and
2) the corresponding algorithms,

to measure the RPO values: d, θ, and φ, while with low-cost implementations of hardware and computations.

C. The Platform Used in This Paper

The platform used in this paper is illustrated in Fig. 2.

III. HARDWARE DESIGN IN THIS PAPER

The hardware module we designed consists of two sub-modules: the beacon module and the receiver module. The beacon module is mounted on the robotic platform, as illustrated in Fig. 2; for abbreviation, the beacon module, with the robotic platform, is called the beacon. The non-beacon robot (or simply called the robot) carries the receiver module, as illustrated in Fig. 3(b).

The microcontroller unit (MCU) used in this paper is Arduino AT Mega 2560 (Flash: 32 Kbytes, RAM: 2 Kbytes, Clock: 20 MHz).

A. The Beacon Module

The beacon module is designed to have the rotational laser-emitting function and the wireless-broadcasting function, and carries the (virtual) reference coordinates (here we only need to designate the positive direction of the x-axis of the reference coordinates).

The beacon module mainly consists of a laser-emitter, a gear motor, a vertical rotational axis, an MCU, and an XBee transceiver connected to the MCU. The laser-emitter is fixed
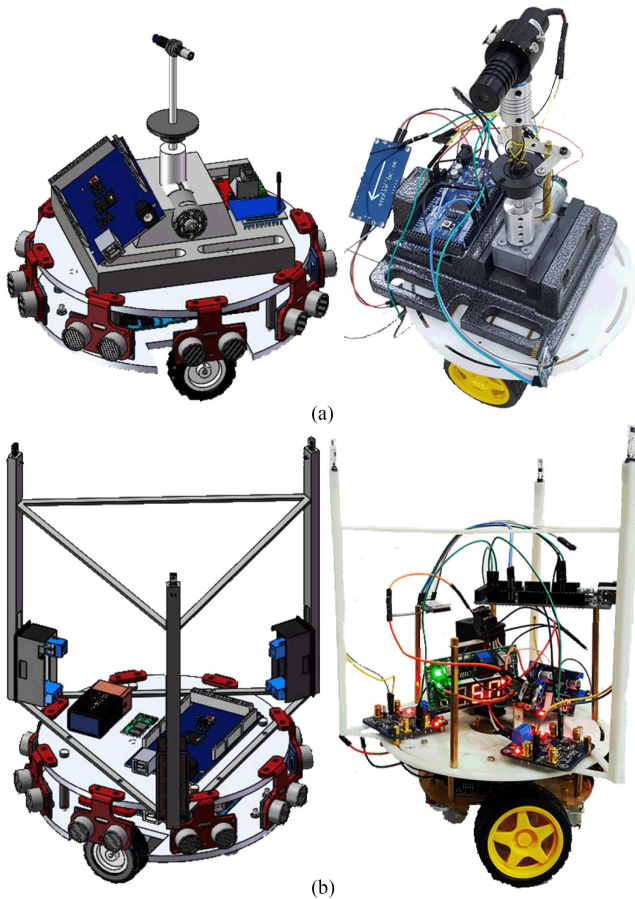
Fig. 3.   The beacon (a) and the non-beacon robot (b). In each of (a) and (b), the left is the CAD model, and the right is the physical hardware.
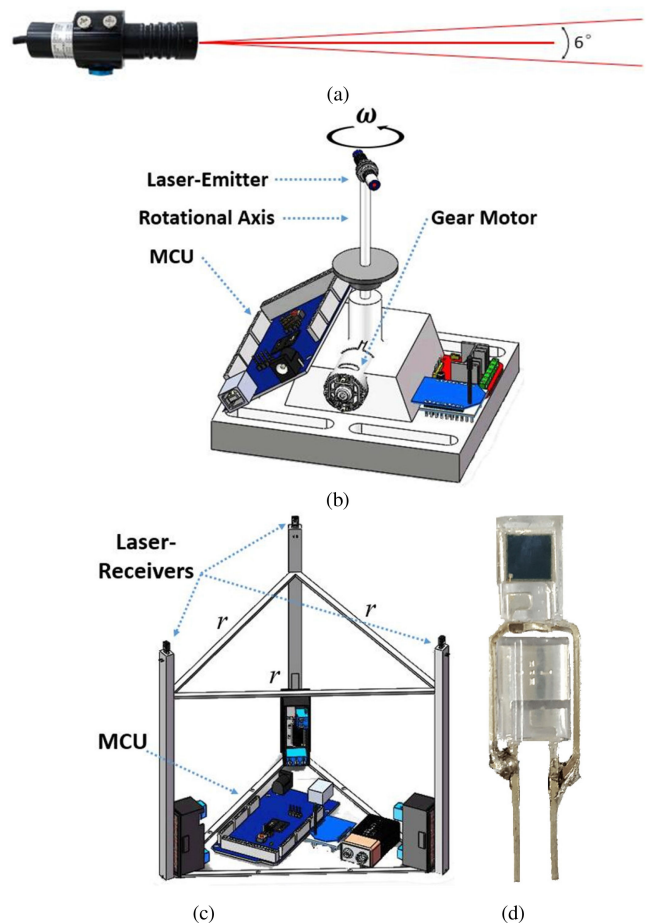

Fig. 4.   (a) The laser-emitter with the scattering angle. (b) The beacon module. (c) The receiver module. (d) The laser-receiver in (c), with no backside.

on the top of the vertical rotational axis, with the laser beam perpendicular to the axis, as illustrated in Fig. 4.

With the control of the MCU, the laser-emitter can rotate at a designated rotational velocity ω with high accuracy, with the range of $\omega \in (0, 10\pi)$ rad/s, the average error per round is less than 0.11% in our hardware setting and thus can be neglected.

In every 360° rotation of the laser-emitter, there is one time that the laser-emitter just points to (or parallels to) the positive direction of the x-axis of the (virtual) coordinates (that is carried by the beacon); for abbreviation, we call this situation the Emitter-Coordinates-Paralleling Event (ECPE). Once the ECPE occurs, an interrupt is triggered and reported to the MCU of the beacon module, and the MCU will then broadcast the current ECPE occurrence to the receiver module using the XBee transceiver (for the details, refer to Section III-C in the following).

B. The Receiver Module

The receiver module, as illustrated in Fig. 4, mainly consists of three laser-receivers, an MCU, and an XBee transceiver connected to the MCU. The laser-receivers form an equilateral triangle with the equal side length (which is denoted as r) and are used to receive the laser signals from the beacon module. Each of the laser-receivers is designed to consist of two silicon photodiodes for the opposite directions, and is able to receive the laser signals in 360°, without backside, as illustrated in Fig. 4(d).

Remark 1: For the possible occlusion concern, since these tiny laser-receivers are arranged *approximately* at the same height of the laser beam, and due to the *scattering angle* of the laser-emitter, as in Fig. 4(a), thus no one will be *practically* blocked by others.

Remark 2: Even for more robots, the possible occlusion can also be avoided as follows: one can arrange the sensors at different heights and use *a multi-beam laser*, *which has a much larger scattering angle* than in Fig. 4(a), the illustration is omitted here.

C. The Wireless Broadcasting Function of the Beacon Module

In every 360° rotation of the laser-emitter, once the ECPE occurs (refer to Section III-A), the MCU of the beacon module will be triggered and the XBee transceiver of the beacon module will broadcast the current occurrence of the ECPE to the receiver modules. To be specific, the XBee transceiver will broadcast a data package about the occurrence of the ECPE, which contains, however, *null information*; and the receiver module will just use the received time of this data package (instead of the content of the data package) to calculate the polar angle (refer to Section IV-C in the following). *So the data for both broadcasting and receiving are very limited, thus with very low-cost and more robust implementations.*
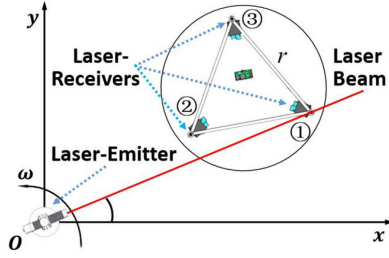
Fig. 5. Illustration of the trigger of the laser-receivers. The red solid line denotes the laser beam.

In addition, the broadcasted data package of the ECPE from the beacon module *does not need to* contain the occurrence time of the ECPE (i.e., the *local* time of the MCU on the beacon), i.e., *there is no need on clock synchronization of the MCUs on different modules, which is another advantage of the hardware design in this paper*.

D. Operating Procedure of the Module in Every Rotational Period

As the laser-emitter in the beacon module rotates at a designated velocity periodically, one can define *the beginning of such a rotational period* of the laser-emitter as the occurrence of the ECPE.

Then, the operating procedure of the hardware in every rotational period is described as follows:

1) Once the ECPE occurs, the MCU of the beacon module will be triggered to broadcast the current occurrence of the ECPE to the receiver module using the XBee transceiver, refer to Fig. 6(a).

2) As the laser-emitter in the beacon module rotates, it will then trigger the laser-receivers in sequence, refer to Fig. 5 and Fig. 6(b).

3) Once a laser-receiver gets the laser signal, an interrupt is triggered to the MCU of the receiver module; the MCU of the receiver module then records the corresponding interrupts from the three laser-receivers, and calculates the current RD relative to the beacon, using the algorithm in Section IV-B.

4) The MCU of the receiver module then calculates the polar angle and its orientation, using the calculations in Section IV-C and Section IV-D, respectively.

In the functions of the modules:

- To measure the RD, we only use the rotational laser-emitting and the laser-receiving functions.
- To measure the polar angle and the orientation, we will use the additional functions: the ECPE and the wireless communication mechanisms.

Remark 3: The ideas of using triangulation for RP or RD measurement are certainly not new, please refer to, e.g., [25] and the references therein; but the existing triangular methods are generally incapable for orientation measurement.

Remark 4: The traditional triangular positioning method is that: send three signals (laser or ultrasonic) to three landmarks with known positions, respectively, and then use the reflected signals to calculate the corresponding three distances to the landmarks, and calculate the position of the signal transceiver using
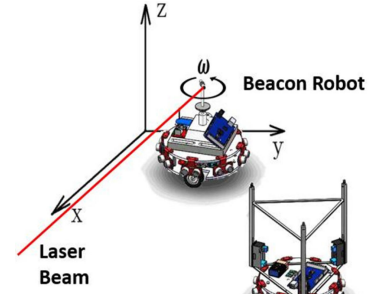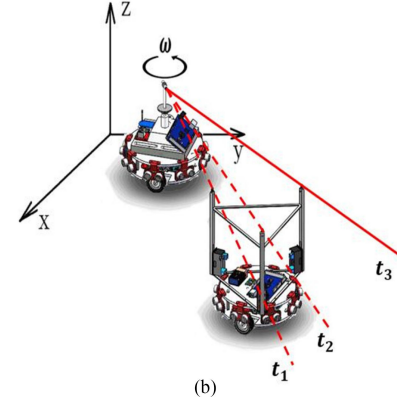
Fig. 6. The operating procedure of the module. (a) Occurrence of the ECPE and message broadcasting. (b) The laser-receivers triggered in sequence.

triangular calculation. One distinct difference of the hardware and the operating in our paper from the traditional positioning methods are that: the laser-emitter and laser-receivers are distributed on two separate sub-modules, and no reflected signals are used.

IV. CALCULATION ALGORITHMS IN EVERY ROTATIONAL PERIOD

The following are the calculation algorithms of the RD d, the polar angle θ, and the orientation φ, respectively. Here d is the RD between the laser-emitter O and the geometrical center C of the laser-receivers.

A. Pose Detection

Denote the laser-receivers triggered in sequence as the receivers 1, 2, 3 (such sequence will be possibly renumbered in the next rotational period of the laser-emitter, depending on the pose of the receiver module relative to the beacon module), denote t_1, t_2, t_3 as the triggered times of the laser-receivers.

Here, we classify the trigger events into two cases (Fig. 7), which difference is that: whether the laser-receiver 2 (which is triggered between other two laser-receivers) and the laser-emitter are located at the same side, relative to the line of the laser-receivers 1 and 3.

B. Calculation Algorithm for the RD

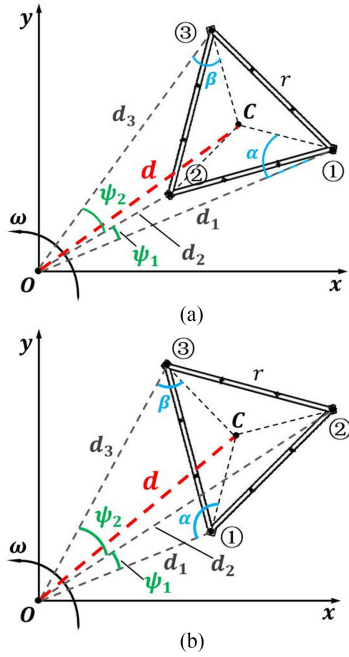For both the two cases, we use the following calculation procedure.

Fig. 7.   (a) *Case I.* (b) *Case II.*

Algorithm 1: Calculation for the RD in Every Rotational Period.

Inputs: Pose detection (Section IV-A) and t_1, t_2, t_3 in this period
Outputs: The RD d in this period

Step 1: Calculate the angles ψ_1, ψ_2 denoted in Fig. 7 as:

$$\psi_1 = \omega(t_2 - t_1),$$
$$\psi_2 = \omega(t_3 - t_2). \tag{1}$$

Step 2: Calculate d_1, d_2, d_3, which are the distances between the laser-emitter O and the laser-receivers 1, 2 and 3, respectively. From triangles $\Delta O13$, $\Delta O12$ and $\Delta O32$, we have the equation array:

$$\begin{cases} d_1^2 + d_3^2 - r^2 = 2d_1 d_3 \cos(\psi_1 + \psi_2), \\ d_1^2 + d_2^2 - r^2 = 2d_1 d_2 \cos \psi_1, \\ d_2^2 + d_3^2 - r^2 = 2d_2 d_3 \cos \psi_2. \end{cases} \tag{2}$$

The solutions can be calculated numerically.
Step 3: Calculate the angles α, β that are denoted in Fig. 7.
Step 4: From $\Delta O1C$ or $\Delta O3C$, we have the RD:

$$d = \sqrt{d_1^2 + \left(\frac{\sqrt{3}}{3}r\right)^2 - 2d_1\left(\frac{\sqrt{3}}{3}r\right)\cos\alpha},$$

or equivalently,

$$d = \sqrt{d_3^2 + \left(\frac{\sqrt{3}}{3}r\right)^2 - 2d_3\left(\frac{\sqrt{3}}{3}r\right)\cos\beta},$$

which is proportional to the value of r.

Remark 5: Notice that the RD $d \neq (d_1 + d_2 + d_3)/3$, because the distances here are the Euclidean-normed scalars, not vectors.

Remark 6: In the above equations, the values of d_1, d_2, d_3 and α, β are different for the two cases:

For *Case I:*

$$d_1 = \frac{r\sin(\pi/3 + \psi_2)}{\sqrt{\sin^2\psi_1 + \sin^2\psi_2 + 2\sin\psi_1 \sin\psi_2 \cos(\pi/3 - \psi_1 - \psi_2)}}, \tag{3}$$

$$d_2 = \frac{r\sin(\pi/3 - \psi_1 - \psi_2)}{\sqrt{\sin^2\psi_1 + \sin^2\psi_2 + 2\sin\psi_1 \sin\psi_2 \cos(\pi/3 - \psi_1 - \psi_2)}}, \tag{4}$$

$$d_3 = \frac{r\sin(\pi/3 + \psi_1)}{\sqrt{\sin^2\psi_1 + \sin^2\psi_2 + 2\sin\psi_1 \sin\psi_2 \cos(\pi/3 - \psi_1 - \psi_2)}}. \tag{5}$$

From $\Delta O13$ in Fig. 7(a), we have

$$\frac{r}{\sin(\psi_1 + \psi_2)} = \frac{d_1}{\sin(\beta + \pi/6)} = \frac{d_3}{\sin(\alpha + \pi/6)},$$

then

$$\alpha = \sin^{-1}\left(\frac{d_3 \sin(\psi_1 + \psi_2)}{r}\right) - \frac{\pi}{6},$$
$$\beta = \sin^{-1}\left(\frac{d_1 \sin(\psi_1 + \psi_2)}{r}\right) - \frac{\pi}{6}. \tag{6}$$

For *Case II:*

$$d_1 = \frac{r\sin(\pi/3 - \psi_2)}{\sqrt{\sin^2\psi_1 + \sin^2\psi_2 + 2\sin\psi_1 \sin\psi_2 \cos(\psi_1 + \psi_2 + \pi/3)}}, \tag{7}$$

$$d_2 = \frac{r\sin(\psi_1 + \psi_2 + \pi/3)}{\sqrt{\sin^2\psi_1 + \sin^2\psi_2 + 2\sin\psi_1 \sin\psi_2 \cos(\psi_1 + \psi_2 + \pi/3)}}, \tag{8}$$

$$d_3 = \frac{r\sin(\pi/3 - \psi_1)}{\sqrt{\sin^2\psi_1 + \sin^2\psi_2 + 2\sin\psi_1 \sin\psi_2 \cos(\psi_1 + \psi_2 + \pi/3)}}. \tag{9}$$

From $\Delta O13$ in Fig. 7(b),

$$\frac{r}{\sin(\psi_1 + \psi_2)} = \frac{d_1}{\sin(\beta - \pi/6)} = \frac{d_3}{\sin(\alpha - \pi/6)},$$

then

$$\alpha = \sin^{-1}\left(\frac{d_3 \sin(\psi_1 + \psi_2)}{r}\right) + \frac{\pi}{6},$$
$$\beta = \sin^{-1}\left(\frac{d_1 \sin(\psi_1 + \psi_2)}{r}\right) + \frac{\pi}{6}. \tag{10}$$

C. Calculation of the Polar Angle

As the beacon module broadcasts the ECPE (refer to Section III-C), the receiver module will receive this signal with a latency τ (the latency depends on the hardware setting, independent from the RD, since the speed of the light is too fast), and the latency can be measured (refer to the Section V). Denote t_r as the time when the receiver module receives the ECPE. Then,
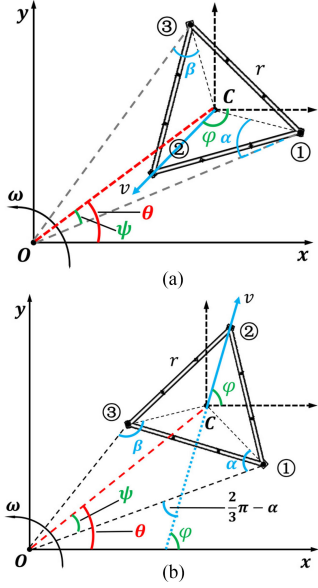
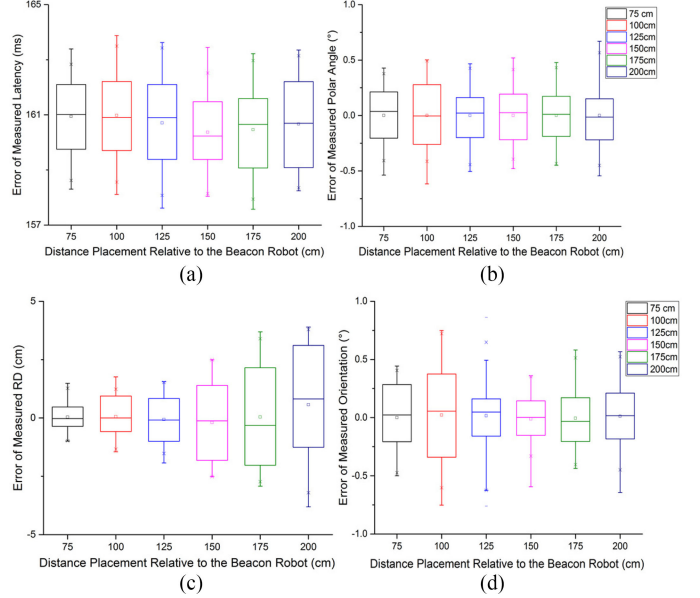Fig. 8. Calculation of the orientation for *Case I* (a) and *Case II* (b).

Fig. 9. (a) Latency τ as a function of the placement distance. (b) Error of the polar angles as a function of the distance. (c) Error of the RDs as a function of the distance. (d) Error of the orientations as a function of the distance.

the polar angle in this rotational period is calculated as:

$$\theta = \omega \left((t_1 + t_2 + t_3)/3 - t_r + \tau \right). \quad (11)$$

In the above calculation, only the local times for the receiver module are used, so there is no requirement on clock synchronization of the MCUs of modules, which is an advantage of our design.

D. Calculation of the Orientation

From Section IV-B, we get the values of α and θ. Denote ψ as the angle in Fig. 8, then,

$$\psi = \omega \left((t_1 + t_2 + t_3)/3 - t_1 \right).$$

1) For *Case I*, the Orientation is:

$$\varphi = \theta - \alpha - \psi - 2\pi/3 = -\alpha - 2\pi/3 + \omega \left(t_1 - t_r + \tau \right),$$

where α is given in (6).

2) For *Case II*, the Orientation is:

$$\varphi = \theta - \psi + (2\pi/3 - \alpha) = (2\pi/3 - \alpha) + \omega \left(t_1 - t_r + \tau \right),$$

where α is given in (10).

That is, we have the calculation of the orientation as follows:

Algorithm 2: Calculation for Orientation in Every Rotational Period.

Inputs: Pose detection (Section IV-A), α, and t_1, t_r in this period, the parameters ω, τ
Outputs: The orientation φ in this period

---

1) For *Case I*, the orientation is:
   $\varphi = -\alpha - 2\pi/3 + \omega(t_1 - t_r + \tau)$,
   where α is given in (6).
2) For *Case II*, the orientation is:
   $\varphi = (2\pi/3 - \alpha) + \omega(t_1 - t_r + \tau)$,
   where α is given in (10).

V. EXPERIMENTS AND ACCURACY OF MEASUREMENTS

In the experiments, we take $\omega = 4\pi \, \text{rad/s}$ (i.e., two rotations per second), in the hardware setting, $r = 20 \, \text{cm}$. We place the robot at different distances, from 75 cm to 200 cm, relative to the beacon, with an increase of 25 cm for each placement. Then, we calculate 100 measurements for each placement. The latency τ is approximately 0.161 second (Fig. 9(a)).

When the laser beam hits on the laser-receivers, it takes 200 μs (the notation μs represents microsecond, $1 \, \mu\text{s} = 10^{-6} \, \text{s}$) for each receiver to switch from a low voltage level to a high voltage level, which is very fast, and thus this latency can be omitted.

The following are the accuracy for the RPO measurements (the calculations of maximum error and average error are denoted in Appendix A):

- *Accuracy of the Polar Angle Measurements*:
  - For the performance of a single measurement, the maximum error is 0.7 degree.
  - The average error is 0.2 degree, as shown in Fig. 9(b).
- *Accuracy of the RD Measurements*:
  - For the performance of a single measurement, the maximum error is 1.8 cm at 100 cm, and 3.9 cm at 200 cm.
  - The average error as 0.8 cm at 100 cm, and 2.3 cm at 200 cm, as shown in Fig. 9(c).
- *Accuracy of the Orientation Measurements*:
  - For the performance of a single measurement, the maximum error is 0.9 degree.
  - The average error is 0.3 degree, as shown in Fig. 9(d).
- *Accuracy of the RP Measurements*:
  - For the performance of a single measurement, the maximum error is 1.8 cm at 100 cm, and 3.9 at 200 cm.
  - The average error is only 0.8% at 100 cm, and 1.2% at 200 cm, as shown in Fig. 10.

IEEE TRANSACTIONS ON VEHICULAR TECHNOLOGY, VOL. 68, NO. 5, MAY 2019

TABLE I
COMPARISON WITH PREVIOUS RESULTS

Method	RP Measurement (at 100 cm)		Orientation Measurement		Capability	Costs		Beacons
	Max. error	Avg. error	Max. error	Avg. error		Hardware	Computation	
This paper	**1.8%**	**0.8% (100 measurements)**	**0.7°**	**0.2° (100 measurements)**	**RPO**	**Low**	**Low**	**One**
[12] [a]	-	1.4% (10000 measurements)	-	-	Only RP	Low	Low	Two
[15]	3%	1% (290 measurements)	-	-	Only RP	High	Low	Multiple
[19]	-	2.6% (300 measurements)	-	-	Only RP	Low	High	One
[20]	<5%	<2% (100 measurements)	19.0°	0.2° (100 measurements)	RPO	Low	Low	One

[a]There is a part of the system that is mounted on the ceiling of the room, with the height 244 cm, the average error is 1.4 cm. To calculate the RP, the polar angle is measured, with the maximum error as 7.7°, and the average error as 1.9° (10000 measurements). No orientation is measured, so the method in [12] can only provide the RP. In [19], the polar angle is measured, with the maximum error as 2.4°, and the average error as 0.3° (300 measurements). No orientation is measured, so the method in [19] can only provide the RP.
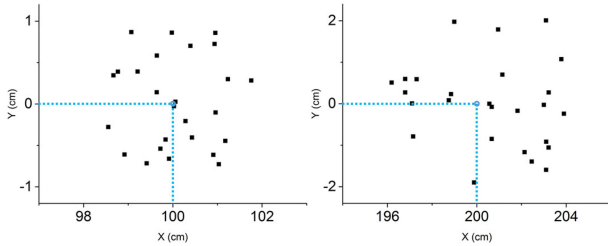

Fig. 10. The RP measurements relative to the beacon for two different placements. The blue circle denotes the placed position of the robot; each black square represents the measured RP.

VI. COMPARISONS WITH OTHER METHODS

A. Main Comparative Aspects and Our Result

This section compares our design with other methods from the following four aspects:
- a) *Measurements Capability*, i.e., for RPO, or only for RP, or RD.
- b) *Accuracy Comparison*, for RP, RD, or RPO (if available in other methods).
- c) *Costs Comparison* (the hardware cost and computational cost).
- d) *Independence Comparison* (i.e., whether a robot can determine its RP or RPO relative to only one beacon, without dependence on other beacons).

The features of our module are that: it can provide higher accuracy for RPO (not merely RP) measurements, while with low-cost implementations on the hardware and computation; moreover, the receiver module can determine its RPO (relative to the only beacon). In addition, there is no necessity on clock synchronization of the MCUs of different modules, which is another feature of our design.

B. Comparison Data

Compared with relevant results, for example, the system designed in [19] can only provide RP measurement, with an average error of 2.6% (2.6 cm at 100 cm), in which the algorithm is also computational intensive. The system designed in [20] has the maximum RPO error above 6%. The system in [17] has lower accuracy and low computational efficiency for RPO measurements. The system in [22] can provide only RP measurement relative to a laser beacon with a lower accuracy. The method in [21] requires multiple beacons. For convenience of reference, Table I lists the comparisons with relevant and comparable results.

C. Difference From the VHF Omnidirectional Range (VOR) Systems

Very High Frequency (VHF) Omni-Directional Range (VOR) is a type of short-range radio navigation system for aircraft, which is used for aircraft to determine their position by receiving radio signals transmitted by a network of ground radio beacons. For the principles of VOR systems: a VOR station sends out an omnidirectional master signal and a directional second signal (by a phased antenna array); by comparing the phase of the second signal with the master signal, the angle or bearing to the aircraft from the station can be determined; the intersection of two lines of positions (or called "radial") from two different VOR stations can determine the position of the aircraft [28].

Compared with the working mechanisms of VOR systems and our design,
1) our design has no phased signal or phase difference used, thus the calculations are different; moreover,
2) in our design, only one beacon is needed.

VII. CONCLUSION

In this paper, we design a hardware module, which has the following distinct features: more measurements capabilities, higher accuracy, and low-cost implementations on hardware and computations, with the use of only one beacon for RPO measurements.

The designed module are mainly used for robots on the plane, due to many planar applications, e.g., in an automatic factory for tasks assistance. For more robots positioning, the possible occlusion can also be avoided by the arrangement of the sensors at different heights and using a multi-beam laser, which has a much larger scattering angle (Remark 2). The design and calculations in this paper form a basis for considering dynamic

positioning between the beacon and the mobile robot (e.g., the robot moves along different trajectories), which will be addressed in a future paper.

There are many future considerations or extensions. For example: 1) Considerations of the hardware malfunctions (e.g., the errors of the laser or the XBee signals), and thus, the design of fault detection and handling functions for more robustness. 2) The computation of the RPO is performed in a deterministic manner, in future, the incorporation of uncertainty will be considered. 3) Design of a module for RPO measurements that is capable for robots on an uneven terrain, possibly using an aerial robot, or using a fusion of some methods. 4) Hardware implementations for formation motion [1]–[3] of mobile robots will also be considered in future.

APPENDIX

Calculation of Maximum Error and Average Error of the Measurements

Denote the n measurements of a value ε as: ε_k, $k = 1, 2, \ldots, n$. Then, the maximum error of the measurements is calculated as $\max(|\varepsilon_k - \varepsilon|)$, where notation $|\cdot|$ denotes the abstract value for a scalar. The average error is calculated as

$$\frac{1}{n} \left| \sum_{k=1}^{n} \varepsilon_k - n\varepsilon \right|.$$

REFERENCES

[1] D. Tick, A. C. Satici, J. Shen, and N. Gans, "Tracking control of mobile robots localized via chained fusion of discrete and continuous epipolar geometry, IMU and odometry," *IEEE Trans. Cybern.*, vol. 43, no. 4, pp. 1237–1250, Aug. 2013.

[2] W. Li, "Notion of control-law module and modular framework of cooperative transportation using multiple nonholonomic robotic agents with physical rigid-formation-motion constraints," *IEEE Trans. Cybern.*, vol. 46, no. 5, pp. 1242–1248, May 2016.

[3] H. Garcia de Marina, B. Jayawardhana, and M. Cao, "Distributed rotational and translational maneuvering of rigid formations and their applications," *IEEE Trans. Robot.*, vol. 32, no. 3, pp. 684–697, Jun. 2016.

[4] J. Wu, X. Yue, and W. Li, "Integration of hardware and software designs for object grasping and transportation by a mobile robot with navigation guidance via a unique bearing-alignment mechanism," *IEEE/ASME Trans. Mechatronics*, vol. 21, no. 1, pp. 576–583, Feb. 2016.

[5] M.-D. Hua, "Attitude estimation for accelerated vehicles using GPS/INS measurements," *Control Eng. Pract.*, vol. 18, no. 7, pp. 723–732, 2010.

[6] L. Li, Y. Liu, K. Wang, and M. Fang, "Estimating position of mobile robots from omnidirectional vision using an adaptive algorithm," *IEEE Trans. Cybern.*, vol. 45, no. 8, pp. 1633–1646, Aug. 2015.

[7] J. Fabian and G. M. Clayton, "Error analysis for visual odometry on indoor wheeled mobile robots with 3-D sensors," *IEEE/ASME Trans. Mechatronics*, vol. 19, no. 6, pp. 1896–1906, Dec. 2014.

[8] R. Carloni *et al.*, "Robot vision: Obstacle-avoidance techniques for unmanned aerial vehicles," *IEEE Robot. Autom. Mag.*, vol. 20, no. 4, pp. 22–31, Dec. 2013.

[9] E. Garcia-Fidalgo and A. Ortiz, "Vision-based topological mapping and localization methods: A survey," *Robot. Auton. Syst.*, vol. 64, pp. 1–20, 2015.

[10] J. Wolf, W. Burgard, and H. Burkhardt, "Robust vision-based localization by combining an image-retrieval system with Monte Carlo localization," *IEEE Trans. Robot.*, vol. 21, no. 2, pp. 208–216, Apr. 2005.

[11] G. Panahandeh and M. Jansson, "Vision-aided inertial navigation based on ground plane feature detection," *IEEE/ASME Trans. Mechatronics*, vol. 19, no. 4, pp. 1206–1215, Aug. 2014.

[12] F. Martinelli, "Robot localization using the phase of passive UHF-RFID signals under uncertain tag coordinates," *J. Intell. Robot. Syst.*, vol. 82, no. 3, pp. 577–593, Jun. 2016.

[13] W. Zhang, X. Yang, and L. Yu, "Sequential fusion estimation for RSS-based mobile robots localization with event-driven WSNs," *IEEE Trans. Ind. Informat.*, vol. 12, no. 4, pp. 1519–1528, Aug. 2016.

[14] N. Deshpande, E. Grant, and T. C. Henderson, "Target localization and autonomous navigation using wireless sensor networks—A pseudogradient algorithm approach," *IEEE Syst. J.*, vol. 8, no. 1, pp. 93–103, Mar. 2014.

[15] U. Yayan, H. Yucel, and A. Yazici, "A low cost ultrasonic based positioning system for the indoor navigation of mobile robots," *J. Intell. Robot. Syst.*, vol. 78, pp. 541–552, 2015.

[16] S. Y. Kim, K. S. Yoon, D. H. Lee, and M. H. Lee, "The localization of a mobile robot using a pseudolite ultrasonic system and a dead reckoning integrated system," *Int. J. Control Autom.*, vol. 9, no. 2, pp. 339–347, 2011.

[17] S. J. Kim and B. K. Kim, "Dynamic ultrasonic hybrid localization system for indoor mobile robots," *IEEE Trans. Ind. Electron.*, vol. 60, no. 10, pp. 4562–4573, Oct. 2013.

[18] L. Marton, C. Nagy, Z. Biro-Ambrus, and K. Gyorgy, "Calibration and measurement processing for ultrasonic indoor mobile robot localization systems," in *Proc. IEEE Int. Conf. Ind. Technol.*, 2015, pp. 131–136.

[19] G. Lee and N. Y. Chong, "Low-cost dual rotating infrared sensor for mobile robot swarm applications," *IEEE Trans. Ind. Informat.*, vol. 7, no. 2, pp. 277–286, May 2011.

[20] J. Pugh, X. Raemy, C. Favre, R. Falconi, and A. Martinoli, "A fast onboard relative positioning module for multirobot systems," *IEEE/ASME Trans. Mechatronics*, vol. 14, no. 2, pp. 151–162, Apr. 2009.

[21] V. Pierlot and M. V. Droogenbroeck, "BeAMS: A beacon-based angle measurement sensor for mobile robot positioning," *IEEE Trans. Robot.*, vol. 30, no. 3, pp. 533–549, Jun. 2014.

[22] S. Hernandez, J. M. Torres, C. A. Morales, and L. Acosta, "A new low cost system for autonomous robot heading and position localization in a closed area," *Auton. Robot.*, vol. 15, pp. 99–110, 2003.

[23] A. Loria, J. Dasdemir, and N. A. Jarquin, "Leader–follower formation and tracking control of mobile robots along straight paths," *IEEE Trans. Control Syst. Technol.*, vol. 24, no. 2, pp. 727–732, Mar. 2016.

[24] Z. Huang, J. Zhu, L. Yang, B. Xue, J. Wu, and Z. Zhao, "Accurate 3-D position and orientation method for indoor mobile robot navigation based on photoelectric scanning," *IEEE Trans. Instrum. Meas.*, vol. 64, no. 9, pp. 2518–2529, Sep. 2015.

[25] J. M. Font-Llagunes and J. A. Batlle, "Consistent triangulation for mobile robot localization using discontinuous angular measurements," *Robot. Auton. Syst.*, vol. 57, pp. 931–942, 2009.

[26] A. F. Paijens, L. Huang, and A. Al-Jumaily, "Mobile robot positioning system for precision manufacturing: The laser lighthouse revisited," in *Proc. Int. Conf. Control Autom. Robot.*, 2017, pp. 91–94.

[27] J. J. M. Lunenburg, S. A. M. Coenen, G. J. L. Naus, M. J. G. van de Molengraft, and M. Steinbuch, "Motion planning for mobile robots: A method for the selection of a combination of motion-planning algorithms," *IEEE Robot. Autom. Mag.*, vol. 23, no. 4, pp. 107–117, Dec. 2016.

[28] M. Kayton and W. R. Fried, *Avionics Navigation Systems*, 2nd ed. New York, NY, USA: Wiley, 1997.

[29] R. P. D. Vivacqua, M. Bertozzi, P. Cerri, F. N. Martins, and R. F. Vassallo, "Self-localization based on visual lane marking maps: An accurate low-cost approach for autonomous driving," *IEEE Trans. Intell. Transp. Syst.*, vol. 19, no. 2, pp. 582–597, Feb. 2018.

[30] A. Fascista, G. Ciccarese, A. Coluccia, and G. Ricci, "Angle of arrival-based cooperative positioning for smart vehicles," *IEEE Trans. Intell. Transp. Syst.*, vol. 19, no. 9, pp. 2880–2892, Sep. 2018.

Xinzuo Wang received the bachelor's degree from Nanjing University, China. He is currently working toward the graduation degree at the University of Virginia, USA. His research interests include autonomous mobile vehicles and wireless sensor networks.

Wei Li (M'14–SM'15) received the Ph.D. degree in automatic control from Shanghai Jiao Tong University, Shanghai, China, in 2008. From 2009 to 2010, he was a Postdoctoral Research Associate with the Department of Electrical Engineering, University of Texas at Dallas, Dallas, TX, USA. Since 2010, he has been an Associate Professor with the Department of Control and Systems Engineering, Nanjing University, China. His current research interests include robotics, autonomous mobile robots, decentralized control, cooperative control of mobile robotic agents, and wireless sensor networks. Dr. Li is an Associate Editor of the *Asian Journal of Control* and a member of the Editorial Board of the *Frontiers in Robotics & AI—Multi-Robot Systems*.